NJC

Accepted Manuscript

This is an *Accepted Manuscript*, which has been through the Royal Society of Chemistry peer review process and has been accepted for publication.

Accepted Manuscripts are published online shortly after acceptance, before technical editing, formatting and proof reading. Using this free service, authors can make their results available to the community, in citable form, before we publish the edited article. We will replace this *Accepted Manuscript* with the edited and formatted *Advance Article* as soon as it is available.

You can find more information about *Accepted Manuscripts* in the Information for Authors.

Please note that technical editing may introduce minor changes to the text and/or graphics, which may alter content. The journal's standard Terms & Conditions and the Ethical guidelines still apply. In no event shall the Royal Society of Chemistry be held responsible for any errors or omissions in this *Accepted Manuscript* or any consequences arising from the use of any information it contains.

ROYAL SOCIETY OF CHEMISTRY

www.rsc.org/njc

Table of Contents

Multi-core MgO NPs@C core-shell nanospheres for selective CO_2 capture at mild condition

Tae Kyung Kim,[a] Kyung Joo Lee,[a] Junhan Yuh,[b] Sang Kyu Kwak[c] and Hoi Ri Moon*[a]

A composite material of 3-nm magnesium oxide nanoparticles embedded in carbon nanospheres showed selective CO_2 adsorption capacity over N_2.

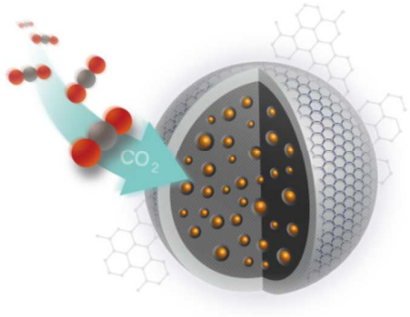

Cite this: DOI: 10.1039/c0xx00000x

www.rsc.org/NJC

PAPER

Multi-core MgO NPs@C core-shell nanospheres for selective CO_2 capture at mild condition

Tae Kyung Kim,[a] Kyung Joo Lee,[a] Junhan Yuh,[b] Sang Kyu Kwak,[c] and Hoi Ri Moon*[a]

Received (in XXX, XXX) Xth XXXXXXXXX 20XX, Accepted Xth XXXXXXXXX 20XX

DOI: 10.1039/b000000x

The core-shell structures have been attracted in catalysis, because the outer shells isolate the catalytically active NP cores and prevent the possibility of sintering of core particles during catalytic reaction at physically and chemically harsh conditions. We aimed to adopt this core-shell system for CO_2 sorption materials. In this study, a composite material of multi-core 3 nm-sized magnesium oxide nanoparticles embedded in porous carbon nanospheres (MgO NPs@C) was synthesized from a gas phase reaction via solvent-free process. It showed selective CO_2 adsorption capacity over N_2, and mild regeneration conditions.

Introduction

The rapid growth of industry causes serious environmental issues, and global warming due to the accumulation of carbon dioxide (CO_2) is a key catalyst for the increasing intensity of natural disasters.[1] Flue gas from coal-burning power plants is a major source for CO_2 emission and technologies for capturing CO_2 from flue gas are needed urgently, which had led to significant interest in this area. Among the various methods to reduce CO_2 emission, its adsorption on solid sorbents is a promising method in terms of a wide range in the operating temperature, less waste production during cycling, and high uptake capacity. Based on the bond strength between the adsorbents and CO_2 molecules, solid sorbents are classified as physisorbent and chemisorbent. Physisorbents are mostly composed of porous inorganic, organic, or hybrid materials, and this group of materials includes zeolites, activated carbons, and metal-organic frameworks.[2,3] On the other hand, solid chemisorbents are metal oxides on which basic sites are largely distributed in order to strongly interact with CO_2 molecules in the acidic nature. Promising candidates in this category are alkaline metal oxides (Na_2O, K_2O),[4] alkaline earth metal oxides (CaO, MgO),[5-8] llithium zirconates,[9,10] and hydrotalcites.[11,12] Ideal adsorbents in practical CO_2 separation and removal processes should exhibit a large uptake capacity, fast adsorption and desorption kinetics, multicycle stability, and a wide operating temperature. However, because the inclusion of all these factors in one material is usually accompanied by a few trade-offs, the search for ideal adsorbent is still under way.

In this study, we synthesized a new composite material of multi-core of 3 nm-sized magnesium oxide nanoparticles embedded in carbon nanospheres (MgO NPs@C) from the gas phase reaction under CO_2 atmosphere. The core-shell structures have been attracted in catalysis, because the outer shells isolate the catalytically active NP cores and prevent the possibility of sintering of core particles during catalytic reaction at physically and chemically harsh conditions.[13,14] We aimed to adopt this core-shell system for CO_2 sorption materials. Especially, as our synthetic process is solvent-free and utilizes CO_2, it is very convenient and environmentally friendly as well. A previous report has described the synthesis of cobalt-carbon core-shell microspheres in a supercritical CO_2 system.[15] Cobalt-carbon core-shell microspheres obtained from this reaction had one cobalt sphere core with a diameter of 1 μm, covered with an amorphous carbon shell with a thickness of ca. 200 nm. In the present work, the gas phase reaction yielded MgO NPs@C composites in which multiple cores of 3 nm-sized MgO NPs were embedded in carbon nanospheres, which is beneficial to CO_2 adsorption. Because MgO NPs with a small diameter have a high surface area to volume ratio, they provide a large number of active sites on the surface for CO_2 interactions, thus allowing for a high CO_2 adsorption capacity, and improved kinetics of formation.[16,17] Many defects on the surface of MgO NPs also lower the temperature for uptake and regeneration of CO_2.[17,18] However, during the adsorption/desorption process, MgO NPs can be sintered and deformed due to significant changes in the crystal structures between MgO (cubic) and $MgCO_3$ (trigonal). In this study, the inert carbon nanospheres enclosing the MgO NPs act as selective channels for CO_2 adsorption compared to N_2. This enhances the stability of embedded MgO NPs by preventing agglomeration as well as side reactions during the CO_2 adsorption/desorption cycles.

Experimental section

Methods and Materials

All chemicals and solvents were of reagent grade and used without further purification. Infrared spectra were recorded with a ThermoFisher Scientific iS10 FT-IR spectrometer. Elemental analyses were performed at the UNIST Central Research Facilities Center (UCRF) in Ulsan National Institute of Science

and Technology (UNIST). Thermogravimetric analyses (TGA) were performed under N_2(g) at a scan rate of 5 ^oC min^{-1}, using a TGA Q50 from TA instruments. X-ray photoelectron spectroscopy (XPS) was performed on a K-alpha from Thermo Fisher. Raman spectroscopy measurements were taken using a micro-Raman system (WITec) with excitation energy of 2.41 eV (532 nm). The chemical composition of MgO NPs@C was analyzed by inductively coupled plasma-mass spectrometry (ICP-MS, PerkinElmer, ELAN DRC-e). X-ray powder diffraction data were recorded on a Bruker D8 advance diffractometer at 40 kV and 40 mA for Cu Kα (λ = 1.54050 Å), with a step size of 0.02º in 2θ. Scanning electron microscopy was carried out on a cold FE-SEM (Hitach s4800). High-resolution transmission electron microscopy (HR-TEM) images and energy dispersive X-ray spectra (EDS) were obtained on JEOL JEM-2100 microscope.

Synthesis of MgO NPs@C

Bis(cyclopentadienyl)magnesium (0.3 g) was placed in the stainless steel reactor lined with alumina vessel under Ar atmosphere, and then the pure dry ice (12 g) was added. The vessel was immediately closed and heated at 350 ^oC and 10 bar for 12 h and then cooled to room temperature. The solid was then washed with mixture solvent of EtOH and water several times and dried at room temperature. A brown-black solid was obtained after filtration.

The crystalline MgO NPs@C were obtained by annealing of magnesium-carbon composite at the 800 ^oC for 2 h in a flowing N_2 atmosphere, heating rate was 10 ^oC/min and flowing rate was 100 mL/min in the tube furnace. The black solid was obtained. Yield: 0.183 g

Etching of MgO NPs@C

MgO NPs@C solid (81.1 mg) was immersed in concentrated HCl 10 mL and stirred at room temperature for 2 h. Black solid product was washed with H_2O and separated by centrifugation for 1.5 h at 7000 rpm (3 times). The product was dried at room temperature under vacuum. Yield: 5.7 mg

Gas Sorption Study

The nitrogen adsorption-desorption isotherms were measured at 77 K by using liquid nitrogen on a BELsorp-MAX. Sorption isotherms for CO_2 and N_2 were also measured at 298 K by using water bath. Prior to adsorption measurement the samples were evacuated at 100 ^oC under vacuum ($p < 10^{-5}$ mbar) for 12 h. The specific surface area was determined from the linear part of the BET equation, and the pore volume was calculated using a BET plot.

CO_2 cycling

Prior to CO_2 gas cycling experiment, the samples were dried at 500 ^oC for 4 h under N_2 atmosphere in the TGA apparatus. CO_2 gas cycling experiments were performed on a TGA Q50 by using a flow of 15% (v/v) CO_2 mixture in N_2, followed by a flow of pure N_2. A flow rate of 60 mL/min was employed.

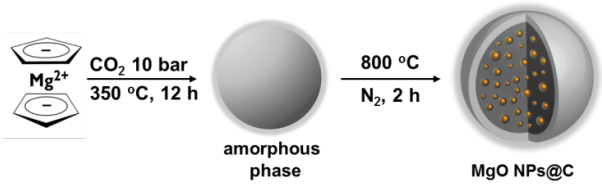

Scheme 1 Schematic illustration of the formation of magnesium oxide nanoparticles embedded in carbon nanospheres (MgO NPs@C).

Results and discussion

As shown in Scheme 1, MgO NPs@C was synthesized from a two-step thermal treatment of bis(cyclopentadienyl)magnesium ($MgCp_2$) under a CO_2 atmosphere. Since $MgCp_2$ is an easily vaporizable organometallic precursor, during the first thermal treatment at 350 ^oC and 10 bar of CO_2, the gas phase of $MgCp_2$ was decomposed and formed a composite of amorphous magnesium and carbogenic species. The successive annealing of the amorphous composite at 800 ^oC under an inert atmosphere yielded the crystalline MgO NPs, which are stabilized in the carbon shell.

TEM images of the resultant dark brown solid before annealing (Fig. 1a) showed a spherical morphology with diameters of ca. 300 nm. Annealing for carbonization of carbon source as well as crystallization of MgO resulted in a black powder, and its scanning electron microscope (SEM) image revealed that it maintained the spherical shape (Fig. 1b). A dark field TEM image showed the multiple cores of MgO NPs embedded in a carbon shell (Fig. 1c). For clear comparison, MgO NPs were etched in an acidic solution to remain the carbon shell only, and its dark field TEM image of resultant inner hollow carbon shell exhibited no bright part corresponded to MgO NPs (Fig. 1d). Elemental mapping for a single nanosphere of MgO NPs@C (Fig. 1e) also revealed that the MgO NPs were well dispersed in the carbon shell. The size of MgO could not be ascertained clearly because of the low electron density of MgO, even in a dark field TEM image. However, calculation of the crystalline size of MgO, estimated by the Debye-Scherrer equation[19] using the (200) reflection of X-ray diffraction (XRD) patterns, indicated the formation of MgO nanocrystals with diameters of 2.9 nm (Fig. 1f). As shown in the XRD patterns, before annealing, the composite was in an amorphous phase, but after annealing, MgO NPs@C was composed of single-phase cubic MgO nanocrystals and a carbon shell, corresponding to JCPDS file no. 89-7746 and a broad peak around 2θ = 24^o, respectively. The chemical composition of the solids was identified using X-ray photoelectron spectroscopy (XPS), by monitoring the Mg 2$p_{3/2}$, C 1*s*, and O 1*s* peaks (Figs. 1g, S1-3 and Table S1). In the amorphous composite before annealing, magnesium in the oxide form (49.3 and 49.8 eV for MgO, 50.6 eV for $Mg(OH)_2$ and $MgCO_3$), a trace of $MgCp_2$ (50.3 eV) and carbogenic species (283.8 eV for graphitic carbon, 284.5 eV for hydrocarbon, 288.9 eV for CO_3^{2-}) were observed (Fig. S1 in the ESI). On the other hand, XPS results of MgO NPs@C revealed two magnesium species in different chemical environments; one was Mg-O in the core of MgO NPs (49.3 eV), and the other was

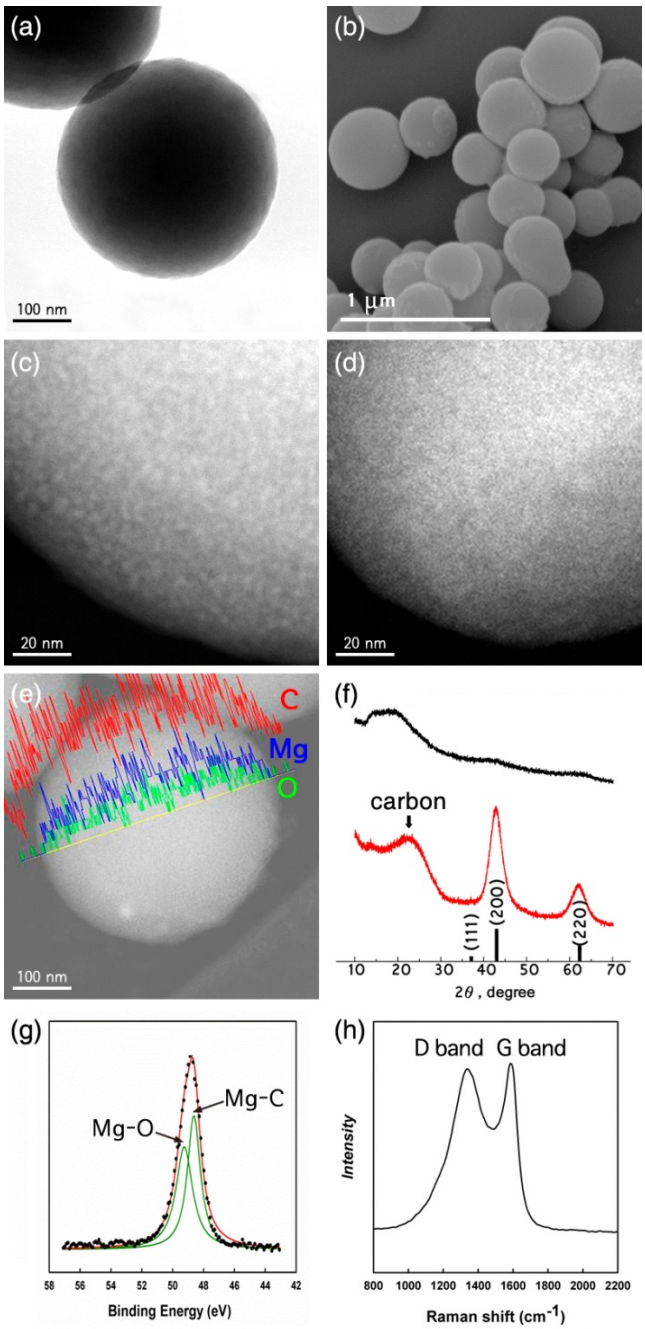

Fig. 1 HR-TEM images of MgO NPs@C for (a) bright field before annealing, (c) dark field after annealing at 800 °C and (d) dark field after etching MgO NPs. (b) SEM image of MgO NPs@C. (e) elemental mapping of a nanosphere of MgO NPs@C. (f) XRD patterns of the solid before annealing (top, black), and MgO NPs@C after annealing (bottom, red). The pattern of MgO@C is indexed as cubic MgO (JCPDS 89-7746). (g) XPS result for Mg $2p_{3/2}$, and (h) Raman spectrum of MgO NPs@C.

Mg-C at the interface between MgO NPs and the carbon shell (48.6 eV) (Fig. 1g). As shown in Fig. 1h, Raman spectroscopy exhibited two peaks at 1339 and 1585 cm^{-1}, which were assigned to the disordered D band and graphitic G band, respectively. This result also demonstrated the formation of a disordered carbon

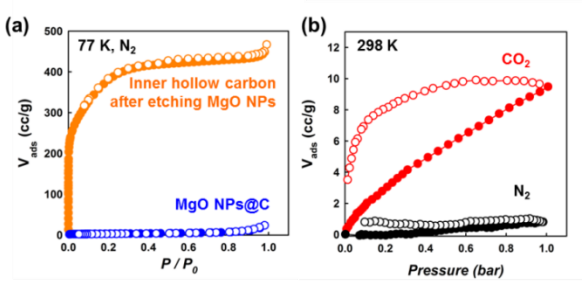

Fig. 2 (a) N_2 gas sorption isotherms of inner hollow carbon shell and MgO NPs@C at 77 K (b) CO_2 and N_2 gas sorption isotherms of MgO NPs@C at 298 K. Filled shapes, adsorption; open shapes, desorption.

shell in core-shell structures. The inductively coupled plasma analysis of MgO NPs@C revealed that the MgO content in the composites was 33 wt% (Table S2 in the ESI).

In order to assess the structure of the MgO NPs@C composite, a nitrogen adsorption-desorption measurements at 77 K were conducted for MgO NPs@C and inner hollow carbon, which were the products before and after etching MgO NPs, respectively. As shown in Fig. 2a, MgO NPs@C showed a typical type II isotherm, characteristic of nonporous materials. However, after etching MgO NPs, inner hollow carbon shell showed very high surface area and pore volume of 1279 m^3/g and 0.72 cc/g, respectively. Its pore size distribution analyzed by the nonlocal density functional theory (NLDFT) algorithm indicated that the MgO NPs filled micropores centered at 0.96 nm as well as mesopores around 2.5 nm in the multi-core MgO NPs@C nancomposite. At 298 K, the carbon shell of MgO NPs@C adsorbed up to 9.5 cc/g of CO_2, whereas there was no uptake of N_2 (Fig. 2b). This implies that the carbon shell selectively permitted the diffusion of CO_2 over N_2. In addition, MgO NPs@C could not be dispersed in water, suggesting they are hydrophobic, unlike bare MgO powder (Fig. S4). This preference of CO_2 over N_2 and H_2O gives MgO NPs@C an advantage as a post-combustion CO_2 capture material, because the composition of flue gas is generally 15% CO_2, 6% H_2O, and 75% N_2.

To exploit the advantages of the small size of MgO NPs protected in carbon nanosphere, we examined the CO_2 gas sorption behaviour of MgO NPs@C. The CO_2 gas cyclic experiments were conducted using a TGA apparatus with a flow of 15% (v/v) CO_2 in N_2, which mimicked dry flue gas. MgO NPs@C absorbed 7.7 wt% CO_2 at 27 °C (Fig. 3a). The CO_2 gas uptake capacity of MgO NPs@C was superior to previously reported adsorbents,[17,20] and was ten times higher than commercially available 50 nm-sized MgO powder (0.76 wt%) (Fig. S5 in the ESI). However, when the CO_2 uptake capacity was compared based on the amount of the active material, the superiority of this multi-core-shell system was firmly established. In the composite, the actual adsorbent, MgO NPs (loading amount, 33 wt%), adsorbed 23.3 wt% of CO_2, which is the high recorded value for MgO nanomaterials under similar conditions. In addition, to examine the operating temperature range, CO_2 adsorption experiments were carried out at 50, 75, 100, 150, and 200 °C (Table 1 and Fig. S6 in the ESI). Upon increasing the

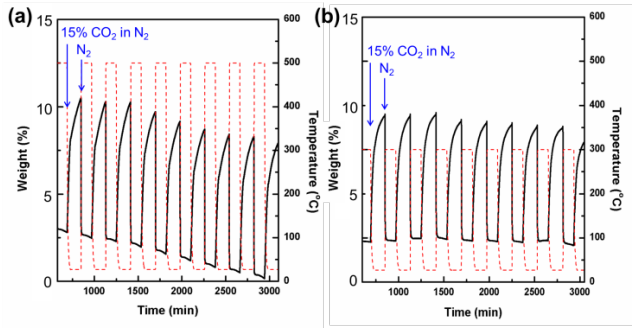

Fig. 3 Study of MgO NPs@C on carbon dioxide gas cycling experiment. Regeneration conditions (a) 500 °C, and (b) 300 °C.

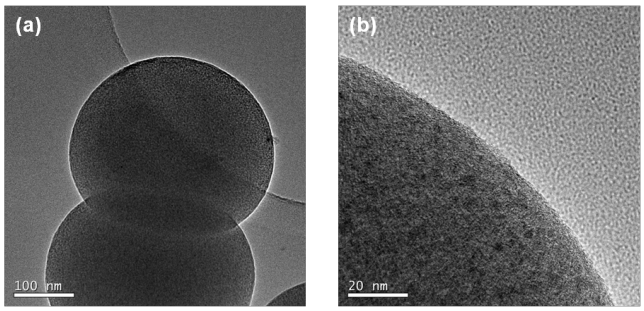

Fig. 4. TEM images of MgO NPs@C obtained after the CO_2 gas sorption cycling experiments. (Regeneration temperature, 500 °C)

adsorption temperature, the total uptake amount was decreased. However since the uptake amount reached ca. 2.0 wt% up to 200 °C, MgO NPs@C can be utilized as a wide range CO_2 adsorbent from room temperature to high temperature. To confirm the effect of carbon shell for CO_2 adsorption behaviour, only inner hollow carbon shell was also tested for the CO_2 gas cyclic experiments in the same conditions (Fig. S7 in the ESI). Since the hollow carbon shell showed 2.4 wt% of the uptake amount at 27 °C, partial adsorption contribution of carbon shell in MgO NPs@C can be expected. However, since even from 75 °C the uptake amount of CO_2 by the carbon shell was negligible, the CO_2 adsorption at high temperatures should be occurred by MgO in the composite.

Because CO_2 molecules are adsorbed on the surface of MgO, nanomaterials derived from it should show a higher CO_2 uptake capacity, but in reality that is not the case always. As shown in a previous study,[17] 5 nm MgO NPs were prepared for CO_2 adsorption, which ultimately adsorbed only 0.7 wt% of CO_2. This might be attributed to the secondary agglomeration of MgO NPs, which results in significant reduction of the active surface. On the other hand, in the present multi-core-shell system, the CO_2-selective carbon shell stabilizes the individual nanoparticles, and thus it maximizes the CO_2 uptake capacity. Furthermore, during nine consecutive cycles of CO_2 adsorption (27 °C)/desorption (500 °C) over MgO NPs@C, there was no significant change in the adsorption capacity. After the cycling experiment, TEM images of MgO NPs@C showed that the spherical carbon shell as well as the small MgO NPs remained intact without any deformation and agglomeration (Fig. 4).

Although high thermal stability of the present MgO NPs@C has several advantages as a high temperature CO_2 sorbent, development of regenerable sorbents at lower temperature is ultimately important in terms of energy consumption. The TGA trace of CO_2-adsorbed MgO NPs@C (Fig. S8) showed that the chemisorbed CO_2 molecules were desorbed from the composites between 200 and 330 °C. This is a very low desorption temperature range, compared to reported value of CO_2 adsorbed on the pure MgO (450 °C).[21,22] Hence, we carried out the CO_2 gas cyclic experiments with MgO NPs@C at a lower regeneration temperature of 300 °C. As shown in Fig. 3b, the total amount of CO_2 adsorbed on MgO NPs@C was maintained at 7.0 wt% for nine cycles, which showed a nearly equivalent capacity compared to the regeneration temperature of 500 °C, along with good cyclability. In addition, the regeneration temperature of 200 °C also provided high CO_2 sorption cyclic properties of 4.2 wt% (Fig. 5). This result suggested that the adsorption strength of the CO_2 molecule on MgO NPs@C was properly modulated, and was not physisorption but weak chemisorption. This might be attributed to the large population of surface defect sites such as surface F-centres and low-coordinate oxygen anions on the 3 nm MgO nanocrystals, which altered the inherent nature of bulk MgO. Furthermore, the carbon shell with selective permeability reduced the competition between CO_2 and N_2, and prevented the formation of side products such as $Mg(OH)_2$ and the sintering of MgO NPs to enable high recyclability.

Table 1 Summary of CO2 sorption capacities of MgO NPs@C

CO_2 adsorption temperature (°C)	Desorption temperature (°C)	Adsorption capacity (%)[a]
27	500	7.7
50	500	5.8
75	500	4.2
100	500	3.4
150	500	2.3
200	500	1.8
27	300	7.0
27	200	4.2

[a] CO_2 gas concentration is 14.95%

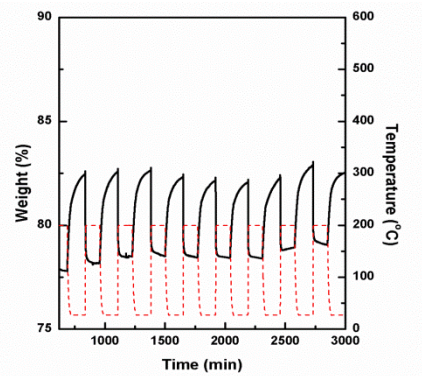

Fig. 5 CO_2 gas sorption cycling results of MgO NPs@C upon adsorption (27 °C)/desorption (200 °C).

Conclusions

Multi-core MgO NPs@C core-shell nanospheres were successfully prepared from the gas phase reaction under CO_2. 3 nm MgO NPs were embedded discretely in the carbon shell, which showed high selectivity for CO_2 over N_2. This composite showed a high CO_2 uptake capacity (23.3 wt% based on MgO amount) as well as high recyclability. MgO NPs@C can be utilized as a wide range CO_2 adsorbent from room temperature to high temperature. More importantly, the regeneration temperature can be lowered by over 200 ^oC while maintaining its CO_2 capacity, compared to common MgO adsorbents. The present MgO NPs@C core-shell composite could be an proper system to take advantage of the superiority of the nanostructured adsorbent.

Acknowledgements

We acknowledge financial support from the Korea CCS R&D Center (KCRC) grant funded by the Korea government (Ministry of Science, ICT & Future Planning) (NRF-2013M1A8A1039968). We also thank Hee Sun Kim for illustrations in scheme and graphical abstract.

Notes and references

[a] *Interdisciplinary School of Green Energy, Ulsan National Institute of Science and Technology, Ulsan 689-798, Republic of Korea. E-mail: hoirimoon@unist.ac.kr*

[b] *New Growth Technology Strategy Department, Corporate Technology Division, POSCO, POSCO center, Seoul 135-777, Republic of Korea.*

[c] *School of Nano-Bioscience and Chemical Engineering, Ulsan National Institute of Science and Technology (UNIST), UNIST-gil 50, Ulsan 689-798, Republic of Korea.*

† Electronic Supplementary Information (ESI) available: Additional information of thermogravimetric analysis trace, TEM, XPS, ICP-MS, Elemental analysis and CO_2 gas sorption results. DOI: 10.1039/b000000x/.

1 K. M. K. Yu, I. Curcir, J. Gabriel and S. C. E. Tsang, *ChemSusChem*. 2008, **1**, 893.
2 D. M. D'Alessandro, B. Smit and J. R. Long, *Angew. Chem. Int. Ed*. 2010, **49**, 6058.
3 J.-R. Li, Y. Ma, M. C. McCarthy, J. Sculley, J. Yu, H-K. Jeong, P. B. Balbuena and H.-C. Zhou, *Coord. Chem. Rev*. 2011, **255**, 1791.
4 K. B. Lee, M. G. Beaver, H. S. Caram and S. Sircar, *AIChE. J*. 2007, **53**, 2824.
5 S. Wang, S. Yan, X. Ma and J. Gong, *Energy Environ. Sci*. 2011, **4**, 3805.
6 L. Li, D. L. King, Z. Nie and C. Howard, *Ind. Eng. Chem. Res*. 2009, **48**, 10604.
7 P.-H. Chang, T.-J. Lee, Y.-P. Chang and S.-Y. Chen, *ChemSusChem*. 2013, **6**, 1076.
8 A. M. Kierzkowska, R. Pacciani and C. R. Muller, *ChemSusChem*. 2013, **6**, 1130.
9 E. Ochoa-Fernández, M. Rønning, T. Grande and D. Chen, *Chem. Mater*. 2006, **18**, 1383.
10 S. Wang, C. An and Q.-H. Zhang, *J. Mater. Chem. A*. 2013, **1**, 3540.
11 N. N. N. A. H. Meis, J. H. Bitter and K. P. de Jong, *Ind. Eng. Chem. Res*. 2010, **49**, 1229.
12 Martunus, Z. Helwani, A.D. Wiheeb, J. Kim and M.R. Othman, *Int. J. Greenhouse Gas Control*, 2012, **7**, 127.
13 S. H. Joo, J. Y. Park, C.-K. Tsung, Y. Yamada, P. Yang and G. A. Somorjai, *Nature Mater*. 2009, **8**, 126.
14 G. A. Somorjai and R. M. Rioux, *Catal. Today* 2005, **100**, 201.
15 J.-s. Yang and Q.-w. Chen, *Chin. J. Chem. Phys*. 2008, **21**, 76.
16 S.-W Bian, J. Baltrusaitis, P. Galhotra and V. H. Grassain, *J. Mater. Chem*. 2010, **20**, 8705.
17 A. M. Ruminski, K.-J. Jeon and J. J. Urban, *J. Mater. Chem*. 2011, **21**, 11486.
18 T. K. Kim, K. J. Lee, J. Y. Cheon, J. H. Lee, S. H. Joo and H. R. Moon, *J. Am. Chem. Soc.*, 2013, ***135***, 8940.
19 B.D. Cullity, Elements of X-ray Diffraction, 2nd ed,; Addison-Wesley: Reading, MA, 1978.
20 S. J. Gregg and J. D. Ramsay, *J. Chem. Soc. A* 1970, 2784.
21 S. Choi, J. H. Drese and C. W. Jones, *ChemSusChem*. 2009, **2**, 796.
22 M. Bhagiyalakshmi, J. Y. Lee and H. T. Jang, *Int. J. Greenhouse Gas Control,* 2010, 4, 51.